Available online at www.sciencedirect.com
ScienceDirect
Journal of Nuclear Materials 358 (2006) 139–150
journal of nuclear materials
www.elsevier.com/locate/jnucmat

Tungsten bronze-based nuclear waste form ceramics. Part 1. Conversion of microporous tungstates to leach resistant ceramics

Vittorio Luca *, Christopher S. Griffith, Elizabeth Drabarek, Harriet Chronis

Australian Nuclear Science and Technology Organisation, Institute of Materials and Engineering Sciences, PMB 1, Menai NSW 2234, Australia

Received 17 January 2006; accepted 26 June 2006

Abstract

The effective immobilization of Cs^+ and/or Sr^{2+} sorbed on hexagonal tungsten oxide bronze (HTB) adsorbent materials has been achieved by heating in air at temperatures in the range 500–1000 °C. Crystalline powdered HTB materials formed by heating at 800 °C displayed leach characteristics comparable to Cs-containing hot-pressed hollandites in the pH range from 0 to 12. If the Cs-loaded HTB sorbents were pressed into pellets prior to calcination, ceramic monoliths could be prepared with negligible Cs volatilization losses. Heating to temperatures in excess of 1250 °C under dynamic air flow resulted in the melting of the sorbent to form phase assemblages consisting of millimetre-sized crystals of bronzoid phases. Up to 5 wt% mass loss was observed for small scale samples of melted materials under dynamic air flow. Both the calcined and melted bronzoid waste forms are multiphase ceramics in which Cs^+ remains bound within, and appears to stabilize, the hexagonal bronze phase, even after complete melting at 1300 °C. The leachability of Sr from the phases prepared by heating appears to be somewhat worse than that of Cs. Saturation of the HTB adsorbents with lanthanide elements (Nd, La, Ce) gave rise to cubic bronze phases in which we propose that the lanthanides substitute at the tungsten or molybdenum sites rather than the tunnel positions. The lanthanides were rather easily leached from the calcined phases in 0.1 M HNO_3 at 150 °C.

1. Introduction

Over the past two decades a significant effort has been under way to develop inorganic ion-exchange materials for isolating specific radioisotopes such as ^{137}Cs and ^{90}Sr from chemically corrosive fission product solutions or radioactive wastes (radwastes) [1–10] and other waste waters [11]. These two isotopes have a relatively short half life of about 30 years but are extremely problematic due to their high solubility and therefore mobility in the environment. In the radwaste context, the ion-exchange strategy has been inspired by the fact that in older radwaste solutions, ^{137}Cs and ^{90}Sr account for a very small fraction of the waste volume but the bulk

* Corresponding author.
E-mail address: vlu@ansto.gov.au (V. Luca).

0022-3115/$ - see front matter
doi:10.1016/j.jnucmat.2006.06.017

of the radioactivity. Concentration of ^{137}Cs and ^{90}Sr onto a small volume of adsorbent potentially allows the bulk of the waste to be disposed of as low-level waste [12]. Once the adsorbent material becomes saturated in these problematic radioisotopes, strategies are required for safe disposition of the resulting small volume of high activity solid. A number of options exist and they include conversion of the adsorbent into glass, ceramic, cementitious or tailored waste forms. In nuclear waste processing, simplicity is key since fewer processing steps implies lower costs, less waste handling and minimized risk.

An elegant solution to the disposition of the saturated adsorbent would be to convert it directly to an acceptable waste form material by a simple thermal process. Inorganic materials which can be used to both partition and immobilize cesium are relatively scarce. This 'cradle-to-grave' approach was first implemented by Dosch [13] who was able to extract the gamut of fission product isotopes and other cationic species onto non-selective titanate adsorbents.

Spurred by a need to simplify waste conditioning by selectively extracting both ^{137}Cs and ^{90}Sr from radwaste, the US Department of Energy (DOE) and collaborating agencies initiated the development of highly selective synthetic crystalline silicotitanate (CST) materials [2,14]. One of these synthetic silicotitanate materials, which has the crystal structure of the mineral sitinakite, has a high selectivity for Cs^+ in acidic and basic solutions, but does not sorb Sr^{2+} from acidic solutions. This means that when targeting acidic solutions such as those that might derive from existing and future spent fuel reprocessing, additional adsorbents need to be employed to extract Sr^{2+}. This implies that an additional waste stream is produced and therefore an additional immobilization problem is created. Disposition of the spent sitinakite was initially to be in glass but new formulations had to be developed to accommodate Ti concentrations in excess of what could be handled by existing formulations [15]. Another approach involved the direct immobilization in the sorbent material itself and it was successfully demonstrated that Cs-loaded sitinakite could be calcined in air to yield waste form materials in which the bulk of the Cs^+ became partitioned into a reasonably durable (leach resistant) $CsTi_2SiO_6$ titanate analogue of the mineral pollucite [16–18]. Despite the fact that the sitinakite adsorbent sorbs both Cs^+ and Sr^{2+} in alkaline solutions virtually no performance data exists for waste form materials derived from silicotitanate ion exchangers saturated with both Cs and Sr.

Recently we reported that microcrystalline hydrated hexagonal tungsten bronze (HTB) materials could be used for the simultaneous adsorption of Cs^+ and Sr^{2+} from acidic solutions [6,19,20] and also provided preliminary results indicating that calcination of the Cs- and Sr-saturated HTB materials in air to modest temperatures in the range 600–1000 °C could yield highly crystalline materials with very low solubility in the pH range from 0 to 12 [21]. In addition it was demonstrated that higher temperatures result in melting which also produces highly durable materials with little or no Cs volatilization.

This study extends our previous initial work with particular emphasis on the simultaneous immobilization of Sr and lanthanide elements.

2. Experimental

The microcrystalline Mo-doped HTB adsorbent and the related pyrochlore material (PYR) used in this work were prepared through pH adjustment of sodium tungstate solutions followed by hydrothermal treatment as previously described [19,22,23]. As prepared materials had typical compositions of $Na_{0.20}WO_3 \cdot H_2O$ for the undoped sample (W–HTB) and $Na_{0.20}Mo_{0.03}W_{0.97}O_3 \cdot H_2O$ for the doped sample (MoW–HTB). Saturation with Cs and Sr was accomplished by contacting the adsorbent with an excess of the metal cation in 1 M HNO_3 solution followed by washing and drying at 70 °C. These Cs- and Sr-saturated materials had typical compositions of $Cs_{0.13}Mo_{0.03}W_{0.97}O_3 \cdot H_2O$ for the Cs-saturated phase (Cs–MoW–HTB) and $Sr_{0.05}Mo_{0.03}W_{0.97}O_3 \cdot H_2O$ for the Sr-saturated phase (Sr–MoW–HTB). When MoW–HTB was saturated with both Cs and Sr using a solution containing both the cations in 1 M HNO_3, typical compositions obtained were $Cs_{0.10}Sr_{0.03}Mo_{0.03}W_{0.97}O_3 \cdot H_2O$. In no case could all the residual Na be removed on saturation with either Cs^+ or Sr^{2+}. This residual Na^+ amounted to a Na/W ratio of about 0.05. Samples were calcined at various temperatures from 500 to 1300 °C. Particle size distributions were measured using a Malvern Mastersizer 2000 laser diffraction particle sizer. For samples heated at 600 and 800 °C particle size distributions were centered at 1.1 and 7.5 μm with a significant fraction of particles around 0.1 μm.

For comparison and bench marking purposes, two Cs–hollandite samples have been used in this

work. A Ti^{3+}-compensated hollandite with formula $Cs_{0.80}Ba_{0.4}Ti_8O_{16}$ (Cs–Ti–Hol) and mean particle size 10 μm was supplied by Cheary [24]. The leaching of this material has been fully described by Luca et al. [25]. An Al^{3+}-compensated hot-pressed hollandite with formula $Cs_{0.10}Ba_{1.0}Al_{2.1}Ti_{5.9}O_{16}$ (Cs–Al–Hol) with mean particle size of 100 μm was supplied by Melody Carter of ANSTO.

Thermogravimetric analyses (TGA) and differential thermal analyses (DTA) were conducted simultaneously on a Setaram TAG24 (France) instrument in flowing air.

X-ray powder diffraction (XRD) patterns were recorded on a Scintag X1 diffractometer employing Cu K_α-radiation and a Peltier detector. In some cases patterns were recorded using a Panalytical X'Pert Pro diffractometer using Cu K_α-radiation and employing a solid state detector utilizing real time multiple strip technology was also used.

Secondary and back-scattered electron images were obtained on a Jeol JSM6400 scanning electron microscope (SEM) operating at 15 keV. Energy dispersive spectroscopy (EDS) analysis of the various phases observed were obtained with a Noran Voyager (Noran) EDS system. Surface area measurements were performed on a Micromeritics ASAP 2010 instrument using nitrogen gas at 77 K.

MCC-1 leach tests [26] were carried out in deionized water and a number of different pH solutions at 90 °C for 7–84 days, using disks that were 10 mm in diameter and 2 mm high. All leaching samples were prepared by machining using non-polar and chemically inert fluids, so pre-leaching was minimized, and the large surfaces of the samples were polished to a 0.25 μm diamond powder finish. Leachate solutions were analyzed using inductively coupled plasma–mass spectrometry (ICP–MS).

Normalized elemental release rates ($g/m^2/day$) were determined according to the relationship

$$NL = \frac{C \cdot V}{F \cdot A \cdot t} \quad (1)$$

where C is the concentration of Cs released to solution, V is the volume of solution, F is the mass of Cs per g of sample, A is the surface area of the sample and t is the time [16]. The value of A is commonly calculated from the geometric area of a polished pellet if a strict MCC-1 protocol is being followed but may be the surface area measured by the BET method if a powdered material is used (PCT). For MCC-1 tests a geometric surface area-to-solution volume $S/V = 0.1\ cm^{-1}$ was used. For PCT tests using powders, volume-to-mass ratios (V/m) of 100 mL/g were employed.

The fraction of Cs released, or elemental loss, f, is defined as $f = (W_0 - W_t)/W_0$ where W_0 is the initial Cs content in the solid phase and W_t is the Cs content remaining in the solid phase after time t. Unless otherwise stated fractional elemental releases from powder materials were determined by loading 0.2 g of powdered sample into a 45 mL Teflon-line autoclave to which was added 20 mL of demineralized water to give a volume-to-mass ratio, $V/m = 100$ (mL/g). The sealed autoclaves were heated in a fan-forced oven in which the temperature was controlled to ±1 °C. The cooled acidic supernatant solutions were filtered through a 0.2 μm filter and analysed by inductively coupled plasma–mass spectrometry (ICP–MS). For experiments in which elemental releases were measured as a function of pH, nitric acid and sodium hydroxide were used to achieve the required pH.

3. Results

3.1. Cs-saturated Mo-doped HTB

A detailed study of the ion-exchange properties of both the undoped (W–HTB) and Mo-doped materials (MoW–HTB) has been reported recently [6] and a preliminary investigation of the immobilization of the sorbed Cs has also been reported [21]. Because the most effective form of the tungstate adsorbent developed to date is that in which some Mo replaces W in the HTB framework [6] we first address the calcination of this phase in air.

The XRD patterns of the dried Cs–MoW–HTB compounds heated to increasing temperatures are shown in Fig. 1. The pattern of the Cs–MoW–HTB has been previously described and is indicative of a poorly ordered material [6]. Calcination of the Cs–MoW–HTB resulted in a narrowing of all reflections in the pattern. By 600 °C (Fig. 1(c)) a strong triplet of reflections appeared that was centered at about 24°2θ. This triplet is due to the monoclinic phase of WO_3 ($P2_1/n$) which has been reported as the most stable tungsten trioxide phase above about 17 °C. Heating to even higher temperatures resulted in an improvement of the apparent crystallinity of the HTB pattern and an increase in the relative intensity of the WO_3 pattern. At temperatures above about 900 °C additional low-angle reflections appeared that were characterized by a series of

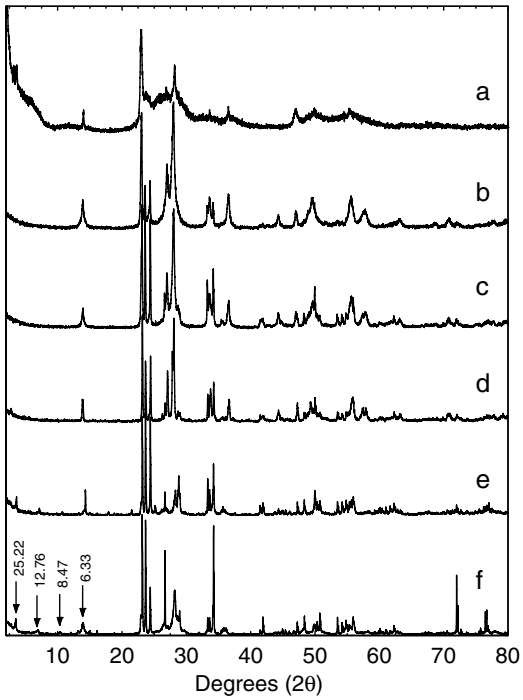

Fig. 1. XRD patterns of Cs–MoW–HTB (a) dried at 70 °C, and calcined at (b) 500, (c) 600, (d) 800, (e) 900 and (f) 1100 °C. Harmonic reflections are indicated by arrows with *d*-spacings also indicated.

harmonic reflections that cannot be unequivocally identified at this time. However, these reflections are reminiscent of intergrowth phases as will be discussed below. The pattern of the bronze phase persisted at all temperatures.

The leaching data of Cs- and Sr-saturated samples heated in air to temperatures in the range 500–1300 °C in 0.1 M HNO_3 for four days are shown in Fig. 2. These aggressive conditions were primarily chosen in order to achieve detectable amounts of Cs in solution in a relatively short period of time. However, it should be noted that the radiolysis of water and air can result in appreciable acidity due to the formation of HNO_3 and therefore the leaching conditions chosen might be relevant to what could conceivably occur in a waste repository where oxic conditions prevail, albeit it at the extreme end. In addition, the use of HNO_3 solutions rather than de-ionized water ensures that the less soluble cations such as Sr and the lanthanides have a greater probability of remaining in solution thus reflecting the true ability of the tungstate matrix to retain these species. In the case of the Cs-saturated material (Cs–MoW–HTB) there was a clear diminution of the fraction of Cs loss in 0.1 M HNO_3 once the calcination temperature exceeded 800 °C, and reached a minimum at 1100 °C. Above this temperature the sample melted and a slight increase in the Cs leachability was observed. From these initial results it was apparent that very low values for the fraction of Cs leached could be achieved for adsorbent materials heated above about 900 °C. By comparison with competing waste form technologies, such as titanates and glasses, these temperatures may be considered exceptionally low. It is important to note that even for the melted sample good performances were maintained even though the sample contains Mo. Synroc formulations do not tolerate appreciable quantities of Mo because of the formation of soluble molybdate species [27]. To overcome this, reducing conditions were used to convert the molybdenum oxides to metal, thus preventing the formation of Cs–molybdates. Thus, the tolerance of the present materials to the incorporation of Mo represents a potentially significant advantage. This will be discussed in greater detail in a subsequent part of this series.

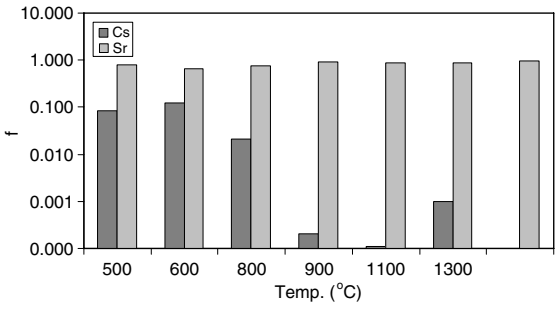

Fig. 2. Fraction of Cs and Sr leached from Cs–MoW–HTB and Sr–MoW–HTB in 0.10 M HNO_3 solutions at 150 °C for 4 days.

The leachability of the Sr–MoW–HTB in 0.1 M HNO_3 was measured after heating samples to temperatures in the range 800–1300 °C and these results are also presented in Fig. 2. While there appeared to be a clear minimum of the leachability for the sample heated at 600 °C, the leachability of Sr was clearly higher than that of Cs for each temperature investigated.

The Cs–MoW–HTB sample heated to 800 °C and the Sr–MoW–HTB sample heated to 600 °C were chosen for more detailed study of the dependence of leaching on pH. These data are shown in Fig. 3 and are compared with Cs leaching from two different types of Cs–hollandite samples which are regarded as the benchmark for durable, ceramic

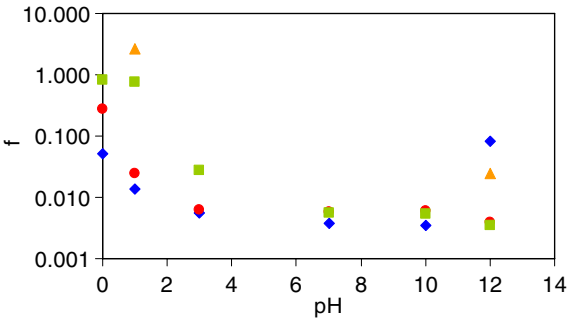

Fig. 3. Leaching of Cs and Sr from powdered waste form materials in solutions of varying pH at 150 °C for 4 days. Cs–Al–Hol (●), Cs–Ti–Hol (▲), Cs–MoW–HTB calcined at 800 °C (◆) and Sr–MoW–HTB calcined at 600 °C (■).

Cs waste forms. In the case of Cs–MoW–HTB, these data demonstrate that these materials are stable across a wide pH range and that the Cs leachability is lower than that of both Cs–hollandite materials under the experimental conditions used, even though the mean particle size of the bronze materials was lower than that of the hollandite sample. It should be emphasized in evaluating this data that the particle size of the Cs–Al–Hol sample was an order of magnitude larger than either the Cs–Ti–Hol or the bronze materials. The pH dependence of the fractional Sr loss from Sr–MoW–HTB in the pH range 3–10 was low and comparable to that of Cs from Cs–MoW–HTB. However, at low pH values the durability of the Sr–MoW–HTB phase was significantly compromised with nearly all of the Sr removed from the heated Sr–MoW–HTB at pH values less than or equal to 1. In comparison, the fractional Cs loss from the Cs–MoW–HTB heated to 600 °C was only about 0.1 at this pH.

XRD patterns of the Sr–MoW–HTB compositions heated at 500 and 600 °C (not shown) evidenced the formation of HTB and monoclinic WO_3 phases. It should be noted that Sr–MoW–HTB samples calcined to such low temperatures have been shown by SEM to be extremely fine grained and porous. Significant crystallinity was only observed for calcination temperatures above about 800 °C. For samples heated at 1000 °C three distinct crystal morphologies with different electron contrasts were observed in the back scattered electron images. Large (10–20 μm) cuboid particles with light contrast analyzed as WO_3 and sometimes contained very minor concentrations of Mo and Sr. Smaller regions of the sample filling the spaces between the WO_3 particles with dark contrast analysed as $Na_{0.58}Mo_{0.73}W_{0.28}O_3$ suggesting that this phase was a cubic bronze. Smaller regions of the sample with intermediate contrast, also found filling spaces between the large WO_3 grains analyzed as $Sr_{0.58}Mo_{0.31}W_{0.50}O_3$. Examination of a number of these particles revealed some variability of the Mo/W ratio but the Sr content was relatively constant.

3.2. Melted Cs-saturated Mo-doped HTB

Calcination at temperatures above about 1200 °C resulted in melting of the Cs–W–HTB and Cs–MoW–HTB samples as well as pyrochlore materials. In some circumstances melting can represent a processing advantage. Regardless of whether the adsorbent materials were doped or not, similar XRD patterns were observed after melting (Fig. 4). The patterns of the single-phase Cs-saturated W–HTB and MoW–PYR dried at 80 °C and after heating to 1300 °C are compared in the plot of Fig. 4. These patterns show that melting results in quite a complex phase assemblage. Bronzoid patterns were easily recognized by comparison with the

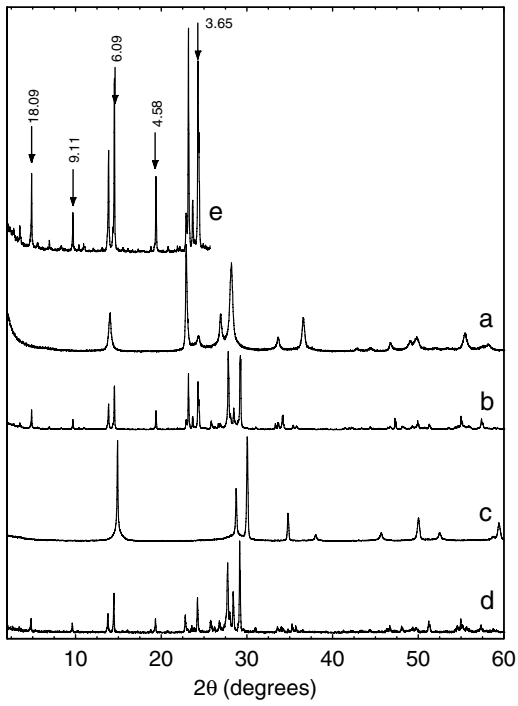

Fig. 4. XRD patterns of (a) Cs-saturated W–HTB dried at 80 °C, (b) sample from (a) melted in air at 1300 °C, (c) Cs-saturated $Mo_{0.1}W_{0.9}$–PYR dried at 80 °C, (d) sample from (c) melted at 1300 °C in air and (e) expanded low-angle region of (b).

unheated bronze phase (Fig. 4(a)) and the presence of multiple reflections around 14°2θ (Fig. 4(b) and (d)) indicated that numerous similar bronze phases with slightly different lattice parameters were present. In addition, the existence of WO_3 and cubic bronze is probable. Additionally, in the low-angle region between 2 and 16°2θ were also present numerous weaker harmonic reflections. Fig. 4(e) shows an expansion of the low-angle region of Fig. 4(b) emphasizing up to five orders of harmonics with the lowest angle reflection occurring at 18.09 Å. Closer scrutiny of this low-angle region also revealed another set of such harmonics with lowest spacing of 31.53 Å. While the complexity of the phase assemblages defies unequivocal interpretation, we surmise that these harmonics are indicative of a number of intergrowth bronze phases.

Examination of SEM cross-sections of these melted HTB and PYR compositions confirmed the presence of several distinct phases. For the Cs–W–HTB sample (Fig. 5) these included a WO_3 composition (phase 1), an $Na_{0.4}WO_3$ composition (phase 2) and several Na- and Cs-containing bronzoid compositions, one having light contrast and a fibrous character (phase 3) and another with dark contrast and irregular morphology (phase 4). In the melted material deriving from the Cs–MoW–PYR a similar XRD pattern was observed (Fig. 5) and indeed similar tungstate phases were also observed by SEM (Fig. 6). Additionally, Na-containing molybdenum tungstates (phase 3, $Na_{0.77}Mo_{0.44}W_{0.44}O_3$) were also observed (Fig. 6). It is interesting to note that as gauged from extensive examination of the sample, Cs partitioned into the tungstate phase containing no Mo. This is potentially advantageous as Cs molybdates are known to be extremely soluble and their existence would have deleterious consequences for the leaching of the samples. Because consolidated blocks could be cut from these melted samples it was possible to conduct an MCC-1 type leaching protocol. Examination of Table 1 confirms that melting HTB or PYR-based compositions containing small concentrations of Mo produced phase assemblages having excellent normalized Cs losses compared with both Cs–hollandite reference materials and undoped Cs–W–HTB.

3.3. Cesium volatility

An important requirement regarding the immobilization of radio cesium in ceramic or glass waste forms is that its volatility on calcination should be minimal. Meeting this requirement minimizes off-gas processing and therefore reduces risk. As an initial step in evaluating the Cs volatility in the bronze waste form system, we analysed the Cs eliminated by collecting the off-gas in a tubular glass reactor. No Cs was detected at temperatures up to about 1100 °C which was the limit of the reactor. Other options for estimating Cs losses are by thermogravimetric analyses and by chemical analysis of Cs-

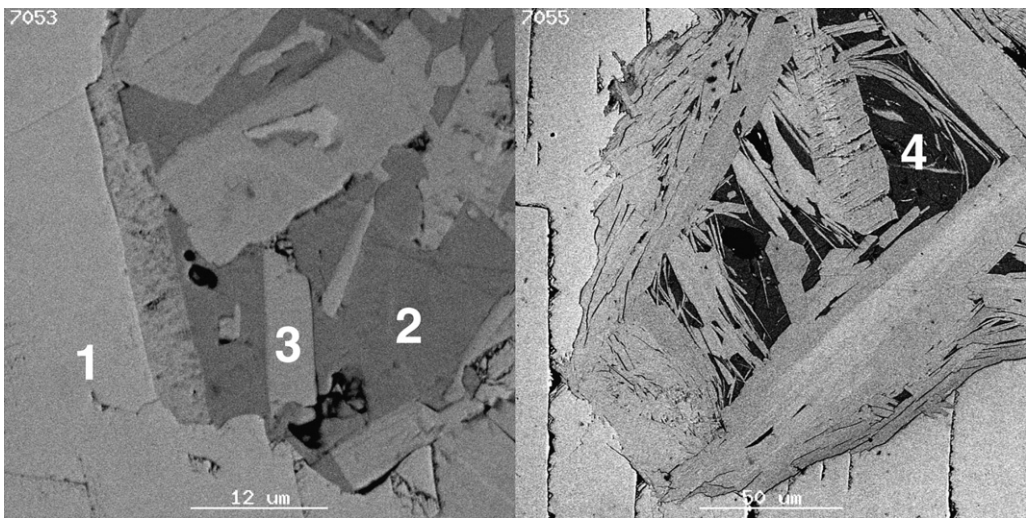

Fig. 5. Cross-sectional images of Cs–W–HTB phase after melting at 1300 °C. Spot EDS analyses were taken at the center of the marks. 1. WO_3, 2. $Na_{0.40}W_{0.99}O_3$, 3. $Na_{0.18}Cs_{0.23}W_{0.95}O_3$ and 4. $Na_{0.22}Cs_{0.24}W_{0.95}O_3$. Seven days Cs leach rate (MCC-1) for this sample was 0.00057 g solid/m^2/g at 90 °C. Left scale bar = 12 μm. Right scale bar = 50 μm.

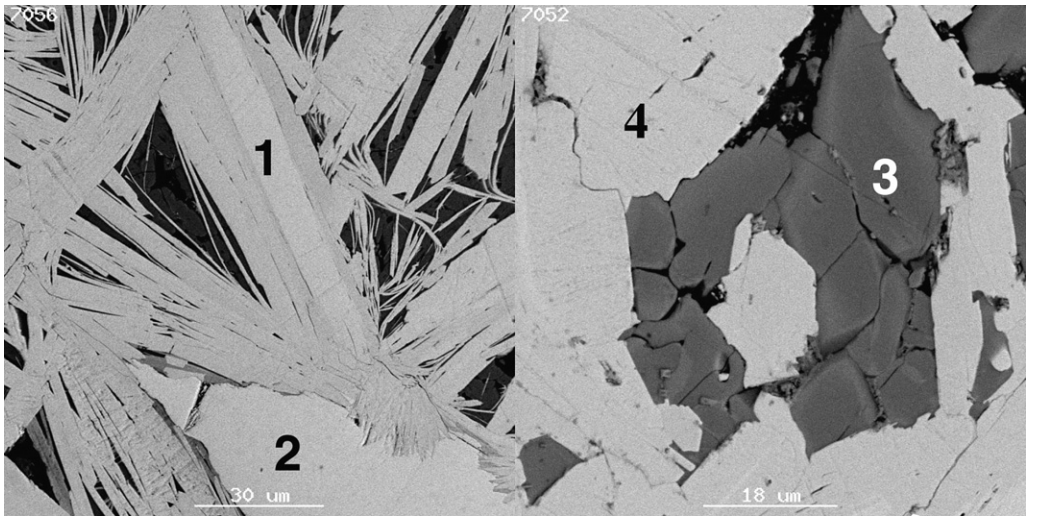

Fig. 6. Cross-sectional images of Cs-saturated $Mo_{0.1}W_{0.9}$–PYR phase after melted at 1300 °C. Spot EDS analyses were taken at the center of the marks. 1. $Na_{0.11}Cs_{0.21}Mo_{0.02}W_{0.96}O_3$, 2. $Mo_{0.01}W_{0.99}O_3$, 3. $Na_{0.77}Mo_{0.44}W_{0.44}O_3$, 4. $Na_{0.22}Cs_{0.24}Mo_{0.04}W_{0.99}O_3$. Seven days Cs leach rate (MCC-1) for this sample was 0.000001 g solid/m^2/g. Left scale bar = 30 μm. Right scale bar = 18 μm.

Table 1
Leaching data for a range of cation saturated bronze and pyrochlore materials

#	Samples	Temp (°C)[a]	Medium[b]	T (°C)[c]	Time (Days)		F[d]	NL[e]
1	Cs–hollandite	HIP	MCC-1	90	7	Cs	0.00042	<0.000001
2	Cs–MoW–HTB	900	MCC-1	90	1	Cs	<0.0001	<0.000001
3	Cs–W–HTB	1300	MCC-1	90	7	Cs	0.00056	0.000057
4	Cs–MoW–HTB	1300	MCC-1	90	7	Cs	0.074	0.0039
5	Cs–MoW–PYR	1300	MCC-1	90	7	Cs	<0.0001	<0.000001
5	Cs, Sr–MoW–HTB	900	HNO_3	150	4	Cs	0.061	0.027
						Sr	0.95	
6	Ce, La, Nd–MoW–HTB	900	HNO_3	150	4	Ce	0.86	0.62
			HNO_3	150	4	La	0.96	0.70
			HNO_3	150	4	Nd	1.02	0.73
7	Cs, Sr, Nd, La, Ce–MoW–HTB	900	HNO_3	150	4	Cs	0.040	0.25
			HNO_3	150	4	Ce	0.64	0.64
			HNO_3	150	4	La	1.04	0.65
			HNO_3	150	4	Nd	1.08	0.67

[a] Calcination temperature.
[b] MCC-1 leach protocol employs a solid polished disk of material cut from the melted mass and demineralized water as the leachant. The concentration of HNO_3 was 0.1 mol/L.
[c] Temperature of leaching reaction.
[d] Fraction of element leached.
[e] Normalized loss in g/m^2/d.

loaded bronze samples containing non-volatile M elements calcined at increasing temperatures. Cs volatility would then be manifest in decreasing Cs/M ratios.

Table 2 shows the Cs/Mo + W elemental ratios for Cs–MoW–HTB phases dried at 80 °C and calcined at 1000 °C. Within experimental uncertainty these results confirmed the result of the off-gas analysis. For the Cs–MoW–HTB doped with a small amount of Zr (Cs–MoWZr–HTB) which is expected to have no volatility at high temperatures, the Cs/Mo + W ratio was also constant within experimental uncertainty. However, a small change in Zr/Cs ratio was indicated. The reasons for this ostensible discrepancy could be that Cs, Mo, and W were volatilized together rather than Cs preferentially.

Table 2
Elemental ratios of selected Cs-saturated Mo-doped HTB adsorbent compositions following calcination at different temperatures

	Sample	Temp.	Cs/Zr	Cs/(W + Mo)
1	Cs–MoW–HTB 306A	80		0.13
2	Cs–MoW–HTB 306B	1000		0.14
3	Cs–MoZrW–HTB 362	80	1.92	0.17
4	Cs–MoZrW–HTB 362A	800	2.01	0.14
5	Cs–MoZrW–HTB 362B	1300	1.52	0.15

Element ratios determined by XRF analysis.

Such a proposition is supported by the thermal analysis which indicated a mass loss of about 6 wt% above 1000 °C (Fig. 7). It should be noted however, that such losses in tiny open crucibles under dynamic air flow as employed during the thermogravimetric analysis does not necessarily imply similar results would be found in larger closed crucibles.

The XRD patterns of the Cs–MoW–HTB samples spiked with ZrO_2 after calcination at 800 °C and melting at 1300 °C are shown in Fig. 8. Unlike the patterns shown for similarly prepared materials in Fig. 4, the patterns of these ZrO_2-spiked materials indicated the presence of a single Cs–MoW–HTB phase with a minor amount of monoclinic WO_3 ($P2_1/n$). Notably, cross-sectional SEM images of the melted sample indicated extensive regions of $Cs_{0.20}Mo_{0.03}Zr_{0.14}W_{0.85}O_3$, minor WO_3 and some unreacted ZrO_2. From these data it was not possible to rule out the possibility that variations throughout the sample might have been due to variability in the Cs content. Because of the relative simplicity of the patterns of the ZrO_2-spiked samples a two-phase Rietveld refinement was successfully conducted.

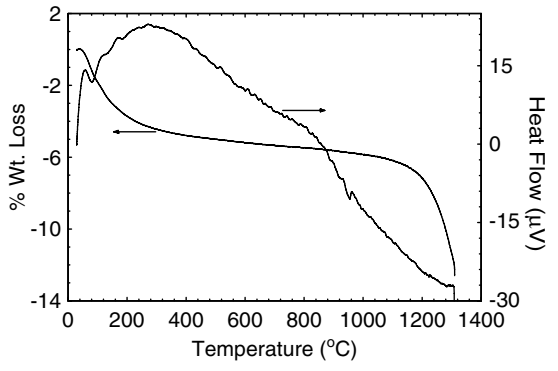

Fig. 7. TGA–DTA trace of Cs-saturated MoW–HTB adsorbent showing mass loss on melting.

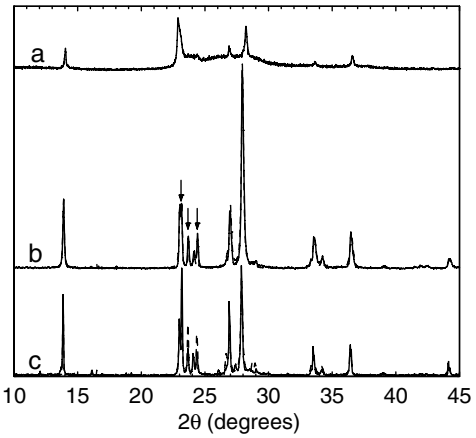

Fig. 8. XRD pattern of (a) air-dried Cs-saturated Zr-spiked MoW–HTB and two-phase Rietveld refinement of sample from (a) calcined at (b) 800 °C and (c) melted at 1300 °C. Arrows mark the position of the triplet of the most intense reflections of monoclinic WO_3.

The refinement was best conducted in the hexagonal space group $P6_322$ in accordance with that employed for $Cs_{0.29}WO_3$ [22]. The pattern of the melted sample was dominated by the Cs-saturated bronze but the refinement was complicated by the presence of additional minor phases.

3.4. CsSr-saturated Mo-doped HTB

When both Cs and Sr were loaded onto the MoW–HTB adsorbent simultaneously and the material heated to 900 °C, the fraction of Cs and Sr leached in 0.1 M HNO_3 over a period of 4 days was 0.07 and 0.95, respectively (Table 1). The value for Cs represented an arguably not significant threefold worsening of the leachability of Cs compared to the Cs-saturated phase while the result for Sr compared with that observed for the pure Sr-saturated phase at the same pH.

The XRD pattern of the CsSr–MoW–HTB is shown in Fig. 9 and both the HTB and triclinic WO_3 structures could be easily identified from the patterns. It was not possible to match some of the very weak features in the experimental pattern of the CsSr–MoW–HTB material to any known phase. Investigation of the cross-sectional SEM (Fig. 10) indicated the presence of three phases in the sample. Phase 1 having composition $Na_{0.03}Cs_{0.22}Mo_{0.03}W_{0.92}O_3$ was consistent with the HTB phase observed in the XRD pattern and contained by far the bulk of the Cs. The phase 2 composition $Cs_{0.005}Sr_{0.002}Mo_{0.04}W_{0.96}O_3$ is consistent with the

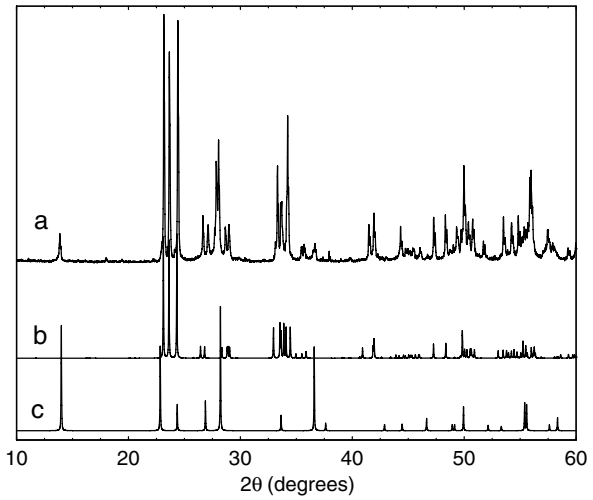

Fig. 9. Experimental X-ray diffraction pattern of (a) Cs- and Sr-exchanged $Mo_{0.1}W_{0.9}$–HTB and simulated patterns for (b) triclinic WO_3 and (c) hexagonal tungsten bronze.

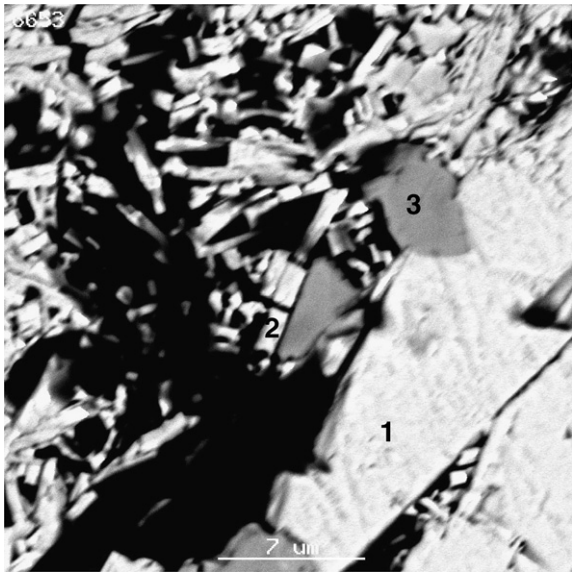

Fig. 10. Cross-sectional image of CsSr-exchanged $Mo_{0.1}W_{0.9}$–HTB phase after calcination at 900 °C. EDS analyses of the various regions are as follows: 1. $Na_{0.03}Cs_{0.22}Mo_{0.03}W_{0.92}O_3$, 2. WO_3, 3. $Sr_{0.51}Mo_{0.07}W_{0.75}O_3$.

perovskite-like triclinic WO_3 that was observed in the XRD while phase 3 has composition $Sr_{0.51}Mo_{0.07}W_{0.75}O_3$ and was the apparent location of all of the Sr. Normally, in tungstate compounds with composition A_xWO_3, a cation the size of

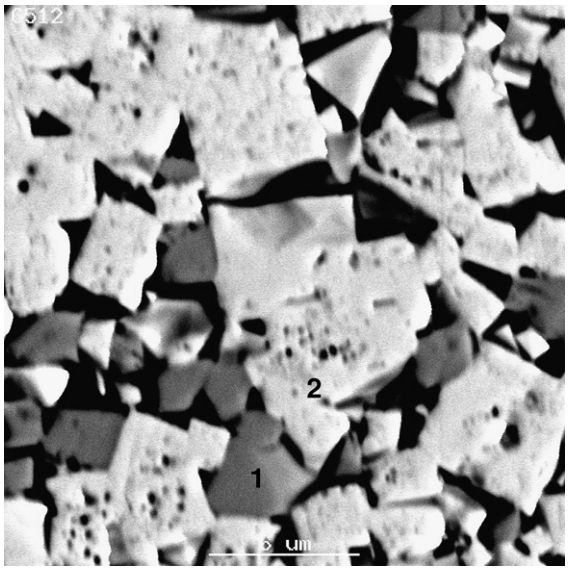

Fig. 11. Cross-sectional image of CeNdLa-exchanged $Mo_{0.1}W_{0.9}$–HTB phase after calcination at 900 °C. EDS analyses of the various regions are as follows: 1. $Na_{0.33}[Ce(IV)_{0.15}Nd(III)_{0.12}La(III)_{0.13}Mo(VI)_{0.\ 23}W(VI)_{0.49}]O_3$, 2. $W_{0.95}Mo_{0.05}O_3$.

Na^+, would be located in either a tetragonal phase for low $x < 0.5$ or a cubic phase for $x > 0.5$. The ICSD database contains no compounds with composition approaching that for this phase. Leaching data for this sample is given in Table 1. The fractional Cs loss and normalized Cs loss were relatively low in 0.1 M HNO_3 while for Sr the values were high as expected.

3.5. Lanthanide-saturated Mo-doped HTB adsorbent

Although the tungsten bronze ion exchanger is selective for Cs^+ and Sr^{2+} against Na^+ it is still capable of sorbing other cationic species from acidic solutions. This raises the possibility that these sorbents could be used to extract a variety of cationic species from radioactive waste solutions, then immobilized through simple calcination in air.

A cross-sectional SEM image of the lanthanide-saturated bronze adsorbent is shown in Fig. 11. Two phases were readily discerned from these images. Angular shaped particles with dark contrast analysed as $Na_{0.33}[Ce(IV)_{0.15}Nd(III)_{0.12}La(III)_{0.13}Mo(VI)_{0.23}W(VI)_{0.49}]O_3$ (region 1) while cuboid shaped particles with light contrast analyzed as $W_{0.95}Mo_{0.05}O_3$ (region 2). The latter phase was the monoclinic tungsten trioxide oxide identified as the

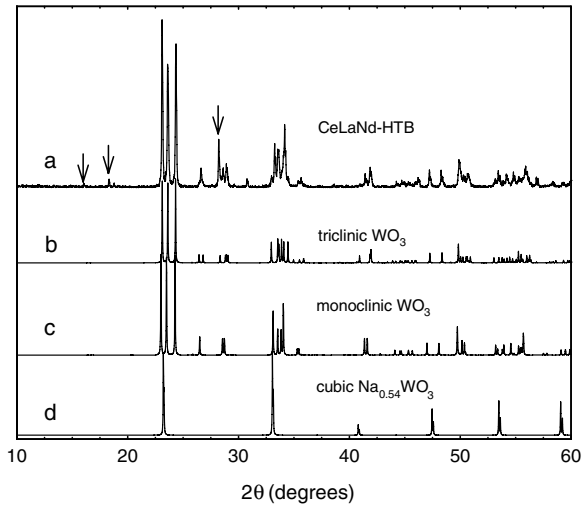

Fig. 12. XRD pattern of (a) Ce, La, Nd-loaded $Mo_{0.1}W_{0.9}$–HTB heated in air at 800 °C compared to simulated patterns for (b) triclinic WO_3, (c) monoclinic WO_3 and (d) $Na_{0.54}WO_3$. Arrows mark positions of a tentative $NaNdW_2O_8$ phase (JCPDS 51-1855).

major component from the XRD pattern (Fig. 12). The lanthanide-containing phase was the minor component as judged from the cross-sectional SEM with the compositional analyses suggesting that this phase was a cubic molybdenum tungstate. These phases each contained significant Na, and since this cation is most likely to occupy tunnel positions, we propose that the lanthanides are substituting for W in the perovskite-like tungsten bronze framework. However, the presence of a cubic lanthanide-containing molybdenum tungstate was difficult to confirm from the XRD pattern shown in Fig. 12 since all the reflections of a cubic phase, if it existed, coincide with many of the reflections of the monoclinic WO_3 phase.

The fractional lanthanide loss from this material was determined in 0.1 M HNO_3 at 150 °C for 4 days and the data are shown in Table 1 (entries 6 and 7). It is apparent that severe leaching of the lanthanides occurs in 0.1 M HNO_3 as was observed for the Sr–MoW–HTB. However, in comparable fashion it can be anticipated that at lower pH values durability should be very good.

4. Discussion

To date very few materials have been described in the literature which can be used for the effective immobilization of ^{137}Cs and ^{90}Sr. These elements are of particular concern in the 0–300 year time frame because of their very high radio toxicity, aqueous solubility and mobility in the geosphere. This is not so much the case for other fission products such as alpha emitting lanthanides and minor actinides. While the latter have extremely long half lives, it has been effectively demonstrated that they are comparatively much more effectively retained during the leaching of waste forms such as glass [28] than are ^{137}Cs and ^{90}Sr. This appears to be due to precipitation, coprecipitation and adsorption on altered glass layers. For the same reasons mobility of these α-emitting isotopes should also be very limited in the environment owing to their tendency to hydrolyse at near neutral pH and precipitate on virtually any available surface.

The main candidate materials for ^{137}Cs immobilization are glass and titanate hollandite prepared by both hot pressing and sintering. While there is a vast body of technological knowledge in the preparation of waste form glasses, it is widely acknowledged that under the mild conditions usually used for testing (de-ionized water at 90 °C) their durability is inferior to that of synroc [29]. After many years of intensive research the leaching of borosilicate glass is now generally well understood particularly for references glasses such as the French R7T7. Such glasses tend to have a very high initial Cs leach rates which plateau over time as the glass-solution interface evolves to eventually form a porous layer of altered siliceous gel material, a zone of material devoid of alkali cations and a dense, relatively impermeable layer at the interface with unreacted glass. This impermeable layer provides a diffusive barrier which limits the alteration rate to a residual value [30,31]. A particularly good example of the phenomenon provided by Advocate et al. [28] who have shown for active as well as inactive glasses that $^{90}(Sr + Y)$ and ^{137}Cs normalized losses reach residual normalized losses of between 1 and 10 g m^{-2} within the first year in pure water.

Materials that can selectively adsorb Cs^+ were first developed in the early nineties and the direct thermal conversion of these Cs-containing adsorbents to potential waste form materials was subsequently demonstrated [17,18]. Highly durable multiphase ceramic powders could be prepared by calcining Cs-loaded Crystalline Silicotitanate (CST) at temperatures between 900 and 1000 °C. The MCC-1 leach rates on pressed pellets were close to zero at these temperatures while lower calcination temperatures consistently gave rise to much higher leach rates. In later work it was demon-

strated that the products of this thermal treatment resulted in phase assemblages consisting of at least three components. These are now known to be SNL-A ($Cs_2TiSi_6O_{15}$) [32] and SNL-B ($Cs_3TiSi_3O_{9.5}3H_2O$) [33] and the Ti analogue of the mineral Pollucite ($CsTiSi_2O_6$) [34]. Only the SNL-A and the pollucite have high leach resistance.

So far there have been no reports of the use of tungsten bronze compounds for the immobilization of radio cesium although Pope et al. [35] have reported on the formation of rare earth cubic bronzes formed from polyoxometallates (arsenates and phosphates) as possible waste form materials. These workers have proclaimed high leach resistance for such phases but as yet have shown no performance data [35–38]. Bessonov et al. [39] have flagged the interesting idea of using lanthanide cubic tungsten bronze materials as Cs transmutation hosts and made mention to durability but again did not provide any performance data.

There is a paucity of Cs–tungsten oxide bronze structures reported in the literature and synthetic procedures have not been widely explored. This study and its predecessor have demonstrated conclusively for the first time that bronzoid materials prepared by aqueous chemical methods can be converted to highly leach resistance phases by simple low temperature thermal treatment. These materials show extremely effective Cs immobilization that is comparable with anything described so far in the literature including Cs–hollandites, glass or CST-derived materials. Their durability with respect to Sr is poorer than for Cs in highly acidic conditions but quite acceptable for intermediate pH values even though these materials are very fine-grained and porous. Therefore, the Sr leach resistance could be expected to be significantly improved by employing higher temperature thermal treatments. At present we have been unable to ascertain the nature of the Sr tungstate phase that is formed on thermal treatment and we expect that this will require a concerted effort to prepare through standard high temperature synthetic methods monophasic materials for structure analysis.

It has also been shown in this study that the simultaneous immobilization of Cs^+ and Sr^{2+} is achievable with little significant change in the effective leach characteristics of the independent Cs- and Sr-waste forms. Lanthanide element immobilization also seems viable with the tungsten bronze system as has been alluded to in the literature with or without incorporation of Cs and Sr. The potential compositional flexibility of the tungsten bronze-based structures has been discussed by Labbe [40] and there seems no reason why many more elements can not be immobilized in such host materials or why other framework elements cannot be incorporated. Addition of further framework elements has the potential to modulate dissolution rates, redox and other properties. We are presently investigating many of these aspects and will be reporting on them in Part 3.

In order to circumvent the formation of soluble cesium molybdates in the production of hollandite from waste feeds containing Mo, it is necessary to employ highly reducing conditions in order to convert Mo to the metallic state [41]. Such redox buffering is achieved by the addition of Ti metal powder. However, this approach can result in the replacement of Al^{3+} compensating cations by Ti^{3+} which has the drawback of oxidation induced leaching [25]. Thus, one important advantage of the present tungstate waste form materials is their ability to handle a certain amount of Mo in the waste feed. This point coupled with the simplicity of the 'cradle-to-grave' concept makes this system a potentially attractive option for the management of certain radioactive waste streams.

It is clear that much investigation remains to be carried out on the tungstate system, especially with regard to the compositional flexibility and tolerance to diverse solution conditions. We take up such issues in a subsequent publication in this series with the aim of achieving a more complete picture of the tungstate based waste form materials.

Acknowledgements

The authors are indebted to Melody Carter of ANSTO for supplying the reference hollandite samples.

References

[1] R.G. Dosch, Sandia National Laboratories, Albuquerque, NM, USA, SAND-80-1212, 1981.
[2] R.G. Anthony, C.V. Philip, R.G. Dosch, Waste Manage. 13 (1993) 503.
[3] A.I. Bortun, L.N. Bortun, A. Clearfield, Chem. Mater. 9 (1997) 1854.
[4] R. Harjula, J. Lehto, Spec. Publ. – Roy. Soc. Chem. 122 (1993) 73.
[5] R. Harjula, J. Lehto, A. Paajanen, L. Brodkin, Nucl. Sci. Eng. 137 (2001) 206.
[6] C.S. Griffith, V. Luca, Chem. Mater. 16 (2004) 4992.
[7] A.I. Bortun, L.N. Bortun, A. Clearfield, Solvent Extr. Ion Exch. 15 (1997) 909.

[8] F. Sebesta, V. Stefula, J. Radioanal. Nucl. Chem. 140 (1990) 15.
[9] T.A. Todd, N.R. Mann, T.J. Tranter, F. Sebesta, J. John, A. Motl, J. Radioanal. Nucl. Chem. 254 (2002) 47.
[10] T.J. Tranter, N.R. Mann, T.A. Todd, F. Sebesta, Czech. J. Phys. 53 (2003) A589.
[11] E.A. Behrens, P. Sylvester, A. Clearfield, Environ. Sci. Technol. 32 (1998) 101.
[12] T.A. Todd, K.N. Brewer, J.D. Law, D.J. Wood, T.G. Garn, R.D. Tillotson, P.A. Tullock, E.L. Wade, Waste Manage. (1997) 2368.
[13] R.G. Dosch, SAND-75-5601, 1975.
[14] R.G. Anthony, R.G. Dosch, D. Gu, C.V. Philip, Ind. Eng. Chem. Res. 33 (1994) 2702.
[15] M.K. Andrews, P.J. Workman, Ceram. Trans. 93 (1999) 171.
[16] M. Nyman, T.M. Nenoff, Y. Su, M.L. Balmer, A. Navrotsky, H. Xu, Mater. Res. Soc. Symp. Proc. 556 (1999) 71.
[17] Y. Su, M.L. Balmer, L. Wang, B.C. Bunker, M. Nyman, T. Nenoff, A. Navrotsky, Mater. Res. Soc. Symp. Proc. 556 (1999) 77.
[18] Y. Su, M.L. Balmer, B.C. Bunker, Mater. Res. Soc. Symp. Proc. 465 (1997) 457.
[19] V. Luca, C.S. Griffith, H. Chronis, J. Widjaja, H. Li, N. Scales, Mater. Res. Soc. Symp. Proc. 807 (2004) 309.
[20] C.S. Griffith, V. Luca, P. Yee, F. Sebesta, Separ. Sci. Technol. 40 (2005) 1781.
[21] V. Luca, E. Drabarek, C.S. Griffith, H. Chronis, J. Foy, Mater. Res. Soc. Symp. Proc. 807 (2004) 303.
[22] K.P. Reis, A. Ramanan, M.S. Whittingham, Chem. Mater. 2 (1990) 219.
[23] K.P. Reis, A. Ramanan, M.S. Whittingham, J. Solid State Chem. 96 (1992) 31.
[24] R.W. Cheary, Acta Crystallogr., Sect. B: Struct. Sci. B47 (1991) 325.
[25] V. Luca, D. Cassidy, E. Drabarek, K. Murray, B. Moubaraki, J. Mater. Res. 20 (2005) 1436.
[26] J.E. Mendel, N.E. Bibler, DOE/TIC-1140.
[27] A.V. Kudrin, B.S. Nikonov, S.V. Stefanovsky, Mater. Res. Soc. Symp. Proc. 465 (1997) 417.
[28] T. Advocat, P. Jollivet, J.L. Crovisier, M. del Nero, J. Nucl. Mater. 298 (2001) 55.
[29] E. Lutze, R.C. Ewing, Radioactive Waste Forms for the Future, North-Holland, New York, 1988.
[30] D. Rebiscoul, P. Frugier, S. Gin, A. Ayral, J. Nucl. Mater. 342 (2005) 26.
[31] D. Rebiscoul, A. Van der Lee, F. Rieutord, F. Ne, O. Spalla, A. El-Mansouri, P. Frugier, A. Ayral, S. Gin, J. Nucl. Mater. 326 (2004) 9.
[32] M. Nyman, F. Bonhomme, D.M. Teter, R.S. Maxwell, B.X. Gu, L.M. Wang, R.C. Ewing, T.M. Nenoff, Chem. Mater. 12 (2000) 3449.
[33] M. Nyman, B.X. Gu, L.M. Wang, R.C. Ewing, T.M. Nenoff, Microporous Mesoporous Mater. 40 (2000) 115.
[34] D.E. McCready, M.L. Balmer, K.D. Keefer, Powder Diffr. 12 (1997) 40.
[35] K. Wassermann, M.T. Pope, M. Salmen, J.N. Dann, H.-J. Lunk, J. Solid State Chem. 149 (2000) 378.
[36] J.M. Pope, E.J. Lahoda, EP 67495, 1982.
[37] M.T. Pope, I.I. Creaser, M.C. Heckel, WO 9401527, 1994.
[38] M.T. Pope, K. Wasserman, WO 0007194, 2000.
[39] A.A. Bessonov, A.M. Fedosseev, J.-C. Krupa, I.B. Shirokova, N.A. Budantseva, J. Solid State Chem. 169 (2002) 182.
[40] P. Labbe, Key Eng. Mater. 68 (1992) 293.
[41] S.E. Kesson, Radioact. Waste Manage. Nucl. Fuel Cycle 4 (1983) 53.